energies

MDPI

Review

Applications of Computational Fluid Dynamics for Mine Ventilation in Mineral Development

Huiuk Yi, Minsik Kim, Dongkil Lee and Jongmyung Park *

Korea Institute of Geoscience & Mineral Resources, 92 Gwahang-no, Yuseong-gu, Daejeon 305-350, Korea
* Correspondence: carl@kigam.re.kr

Abstract: In this paper, the application status of computational fluid dynamics (CFD) modeling in mine ventilation is presented by reviewing papers published since the year 2000. The aspects covered in these papers are the numerical analyses of working faces, mine tunnels, ventilation systems, and open-pit mines. CFD modeling procedures for mine ventilation are summarized. Further, building geometries, grid generation, solutions of equations, model validation, grid-independence studies, and solution convergence are discussed. Several examples of CFD modeling for mine ventilation are provided. Finally, conclusions including recommendations for future studies that may allow for more advantageous applications of such numerical simulations are provided.

Keywords: mine ventilation; computational fluid dynamics; working faces in mines; mine tunnels

Citation: Yi, H.; Kim, M.; Lee, D.; Park, J. Applications of Computational Fluid Dynamics for Mine Ventilation in Mineral Development. *Energies* **2022**, *15*, 8405. https://doi.org/10.3390/en15228405

Academic Editors: Rajender Gupta and Tianhong Duan

Received: 3 September 2022
Accepted: 7 November 2022
Published: 10 November 2022

1. Introduction

Ventilation in the tunnels or working faces of mines serve two primary functions. First, main fans or auxiliary fans must provide mining workers with fresh air. Second, fans or scrubbers should eliminate or reduce hazardous gases and harmful dust. To accomplish these objectives, well-designed tunnels, ducts, and ventilation systems are required. However, data collection via experimental methods is typically difficult, expensive, and time consuming. Computational fluid dynamics (CFD) provides resolutions and details that are better to those obtained via actual measurements in a mine. However, one of the disadvantages of CFD is the difficulty in predicting turbulence. Nevertheless, advances in computers and turbulence modeling are expected to address this problem.

Numerical simulations are powerful tools to analyze and design mine ventilation systems. This review presents data collected since the year 2000 for the analysis of mine ventilation. The overall purpose of this discussion is the analysis and design of mine ventilation systems using CFD.

The computational papers presented in this article provide new information on mine ventilation, which is significant in mining environments such as mining faces, mine tunnels, and open-pit mines. Using CFD, new designs of airflow ducts, mine tunnels, and ventilation systems can be realized. The purpose of this paper is to review CFD in terms of its academic and industrial applications to mine ventilation. Therefore, the body of this paper comprises two sections, i.e., an introduction to CFD (Section 2) and applications of CFD to mine ventilation (Section 3). In Section 2, governing equations, the finite volume method, CFD codes, turbulence models, modeling procedures, model convergence, gas dispersion, dust motion, and fluid age are presented. In Section 3, ventilation at the working faces of mines; mine ventilation in mine tunnels and galleries; CFD applications in open-pit mines; and mine ventilation systems consisting of fans, dust collectors, and ducts are reviewed.

2. Numerical Simulations: Computational Fluid Dynamics

CFD is a powerful tool used to analyze heat and fluid flow. It has been used by numerous academic researchers and industrial professionals to investigate the flow around cars,

ships, airplanes, and so on. Several studies have also been conducted on mine ventilation, froth flotation, groundwater pollution remediation, and oil and gas processes to develop mineral resources. Thus, the role of CFD in these areas has become increasingly important.

2.1. Governing Equations in CFD

The conservation laws in physics require the conservation of mass, momentum, and energy. To satisfy these laws, the continuity equation for mass conservation was expressed by Anderson as follows [1].

$$\frac{\partial \rho}{\partial t} + \nabla \cdot (\rho \vec{V}) = 0$$

where ρ denotes the fluid density, t denotes the time, and V denotes the velocity.

For momentum conservation, the Navier–Stokes equations are expressed as follows. Claude-Louis Navier first introduced the concept of friction using a mathematical expression of the Euler equation, and George Gabriel Stokes further completed this equation [1,2].

$$\rho \frac{\partial \vec{V}}{\partial t} + \rho (\vec{V} \cdot \nabla) \vec{V} = -\nabla p + \rho \vec{g} + \nabla \cdot \tau_{ij}$$

where p denotes the pressure, and τ denotes the viscous stress.

For energy conservation, the energy equation is written as

$$\frac{\partial (\rho i)}{\partial t} + \nabla \cdot (\rho i \vec{V}) = -p \nabla \cdot \vec{V} + \nabla \cdot (k \nabla T) + \Phi + S_i$$

where i denotes the internal energy, k denotes the thermal conductivity, T denotes the temperature, Φ denotes the dissipation function, and S_i denotes a new source term. Detailed definitions of these terms can be found in a paper authored by Versteeg and Malalasekera [2].

2.2. Discretization: Finite Volume Method

The definition of "discretization," which is considered a complex concept, has been simplified by Anderson [1]. Analytical solutions present continuous variations in dependent variables, whereas numerical solutions provide the values of discrete points referred to as grids or meshes. The three methods of discretization are as follows: the finite difference method(FDM), finite element method (FEM), and finite volume method (FVM).

The FVM is often employed in CFD to solve problems. This method is based on the integral form of partial differential equation [3]. Particularly, the Semi-Implicit Method for Pressure-Linked Equations algorithm is used to calculate the pressures and velocities in momentum equation [2,3]. Most commercial simulation software, including ANSYS FLUENT, ANSYS CFX, and STAR-CCM+, employ the FVM for discretization programming. The COMSOL Multiphysics program is based on the FEM.

2.3. CFD Codes

The commercial software ANSYS FLUENT, ANSYS CFX, and STAR-CCM+ yield good results for heat and fluid flow. The FLUENT software [4] has remained popular for several years, as evidenced by its wide applications in numerous studies. Particularly, the availability of data is an advantage of using the FLUENT software. ANSYS CFX [5] is an additional CFD program used for solving the heat and fluid flow in all industrial fields. STAR-CCM+ and Cradle SC/Tetra [6] are excellent solvers of fluid flow problems. OpenFOAM [7] is a free solver for heat and fluid flow problems. Unlike commercial codes, open-source programs are cheap and accessible; hence, this is an emerging area for CFD codes. FLOW-3D [8] is another program with an ability to solve free surface problems. Certain special codes have also been developed for fire analysis. COMSOL Multiphysics is an excellent tool for various engineering problems including fluid flow.

2.4. Turbulence Models

Notably, the selection of appropriate turbulence models to solve problems is critical. Popular turbulence models include the Reynolds-averaged Navier–Stokes (RANS) model, large eddy simulation (LES), and direct numerical simulation (DNS) [2]. When Navier–Stokes equations are time averaged, a new term for the Reynolds stress is created. To close the governing equations, this term should be modeled based on reasonable assumptions. For the k–ε and k–ω models, which are widely applied to engineering problems, this term is modeled using the eddy viscosity. The primary advantage of the k–ε model is the availability of validation data; however, its disadvantages include poor prediction of strong separation cases. Menter [9] proposed the shear-stress transport (SST) k–ω model, which uses k–ε and k–ω for the freestream and near-wall region, respectively. This model demonstrates reasonable accuracy for a wide range of flows. When an appropriate turbulence model cannot be identified, the initial choice of the SST k–ω model is recommended. The LES focuses on large eddies, whereas eddies smaller than the grid size are neglected. The LES has been applied to various engineering problems; however, determining the correct grid size is often difficult. In the LES, larger eddies are directly solved while smaller eddies are modeled using a subgrid scale model. The DNS directly solves the governing equations without using any turbulence model. This implies that the corresponding computation is time consuming and expensive. To date, simple geometries have been applied to the DNS. However, the rapid development of computers is expected to further widen the application scope of the DNS.

In addition to the abovementioned models, the Spalart–Allmaras model is widely used in the aerospace industry. The Reynolds stress model is suitable for strong swirls; however, obtaining converged solutions based on this model is often difficult. The V^2F turbulence model, based on the k–ε model, provides more accurate predictions. A detached eddy simulation is an alternative to the LES, and it uses the RANS model in near-wall regions.

As stated, selecting a correct turbulence model is critical for obtaining exact solutions. Usually, one of the Spalart–Allmaras, k–ε, or SST k–ω models is initially selected as the turbulence model owing to their speed and ease of use. The obtained results are then compared with the experimental data. When the difference between the experimental and numerical data is within an acceptable error range, the selected turbulence model is deemed suitable. When the difference exceeds the acceptable error range, other turbulence models or grids are considered to minimize the errors.

2.5. Procedures of CFD Modeling

The CFD modeling procedure comprises three steps, namely geometry building, grid generation, and equation solving. Figure 1 presents the CFD modeling procedures proposed by Kim et al. [10]. First, the geometry of the flow regions is defined and created. Particularly, geometry-building programs include DesignModeler, SpaceClaim, Gambit, Auto computer-aided design (CAD), Creo, and CATIA. The results of general 3D CAD programs are imported into grid-generation programs using formats such as IGS or STEP. After constructing the geometries, calculation grids are generated. Here, grid-generation programs include FLUENT meshing, ANSYS meshing, ICEM-CFD, and TurboGrid. In particular, ICEM-CFD can generate hexahedral grids with various geometries. When such grids are created, grid information is transferred to solvers such as FLUENT, CFX, and STAR-CCD. The governing equations are obtained by solver codes, and the results are output using postprocessors, such as TECHPLOT, FIELDVIEW, and CFD-POST.

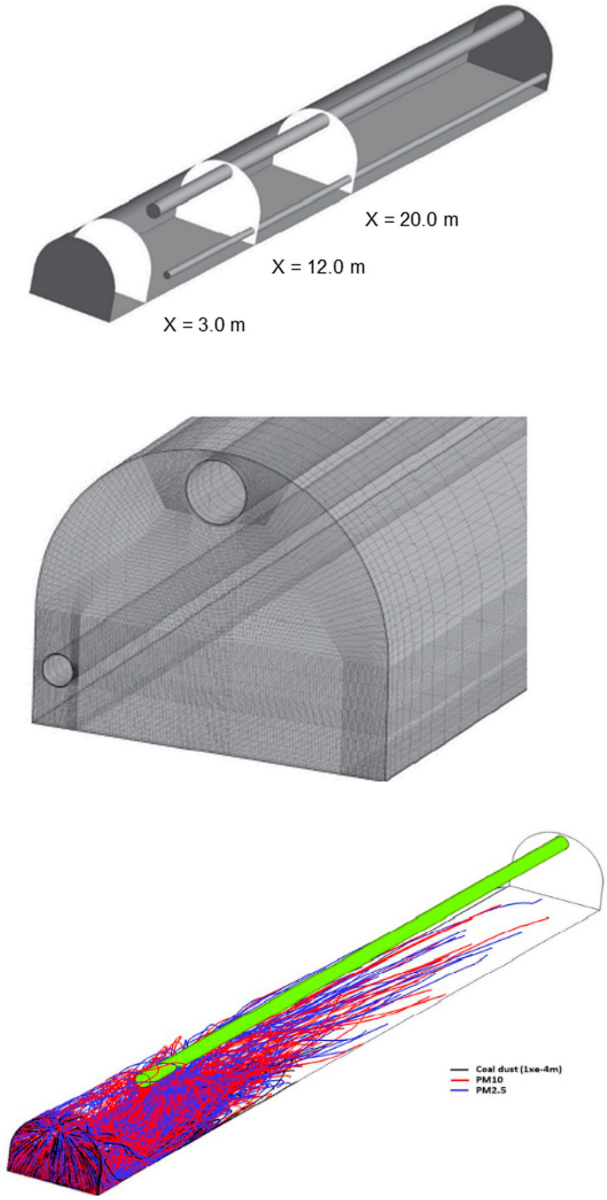

Figure 1. CFD modeling procedures: geometry building, grid generation, solving, and post-processing [10]. (Adapted with permission from ref. [10]. Copyright 2020 Springer Nature Switzerland AG).

2.6. Convergence, Grid-Independence Test, and Validation

2.6.1. Convergence

The convergence of numerical simulation results is usually determined using scaled residuals for the continuity, momentum, energy, and turbulence equations. The total residuals used to determine the imbalance within equations for the conservation of any given variable are obtained over all computational grids. The default range of criteria for the scaled residuals is approximately 10^{-4}–10^{-6}. When all the scaled residuals are below these values, solutions converged through iterations are obtained.

2.6.2. Grid-Independence Test

Usually, the obtained CFD results must be independent of the density and resolution of the calculated grid. To that end, coarse, medium, and fine grids are tested to demonstrate their independence. This step is critical because the uncertainty in CFD results for heat and fluid flow decreases with the optimal grid density and resolution. In addition, the first grid

point near the wall is important in the absence of a wall function. Notably, a value of $Y^+ < 1.0$ is recommended.

2.6.3. Validation

To verify a computational model, a comparison between the experimental and numerical data is recommended. The CFD model is tested and modified based on this validation method. Figure 2 presents a comparison between numerical and experimental results at three calculation planes, as obtained by Parra et al. [11]. Here, the experimental velocities "E" and numerical velocities "N" are compared at different locations in a mine gallery. The velocities are measured using a hot-wire anemometer. The Spalart–Allmaras model is used as the turbulence model for numerical calculations. The difference between the numerical and experimental results is less than 20%. After a comparison between the numerical and experimental data for one duct (blowing), various types of blowing and exhaust ducts are simulated using CFD. The process of comparing the numerical and experimental data for simple geometries validates the analysis of the flow physics of complex geometries.

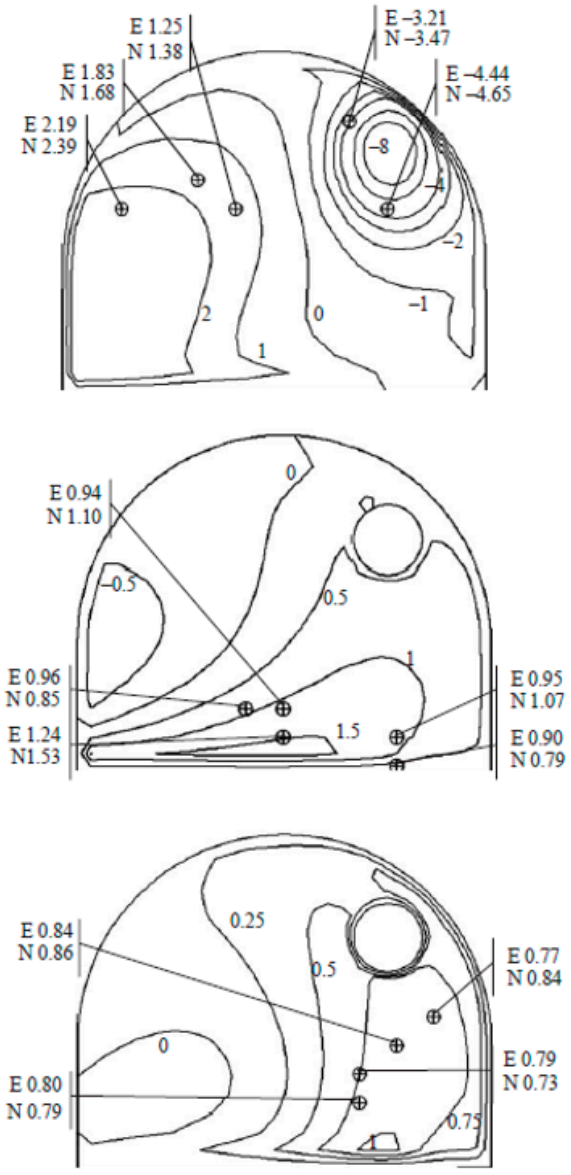

Figure 2. Comparison of numerical and experimental results of streamwise velocities (m/s) for validation of CFD models [11]. (Reprinted with permission from ref. [11]. Copyright 2005 Elsevier Ltd.).

Such validation involves determining the difference between the experimental and numerical data obtained for the base geometry. This difference should be minimized by verifying and developing the geometries, grids, boundary conditions, and turbulence selection of the CFD model. This process validates the optimal designs or parametric studies.

2.7. Governing Equations for the Dispersion of Hazardous Gases in CFD

To investigate the dispersion of gases in underground mines, species transport equations must be solved. The equations for the *i*th species are as follows [12]:

$$\frac{\partial}{\partial t}(\rho Y_i) + \nabla\cdot(\rho\vec{v}Y_i) = -\nabla\cdot\vec{J}i + R_i + S_i$$

where Y_i denotes the mass fraction of each species, R_i denotes the net rate of production of species i, and S_i denotes the production rate obtained by addition from any source. J_i denotes the diffusion flux of species i and is defined as follows for turbulent flow:

$$\vec{J_i} = -\left(\rho D_{i,m} + \frac{\mu_t}{SC_t}\right)\nabla Y_i - D_{T,i}\frac{\nabla T}{T}$$

where $D_{i,m}$ denotes the mass diffusion coefficient for species i, μ_t denotes the turbulent viscosity, SC_t denotes the turbulent Schmidt number, $D_{T,i}$ denotes the thermal diffusion coefficient, and T denotes the temperature.

The diffusion flux J_i consists of laminar and turbulent components. Notably, for turbulent flows, the turbulent viscosity affects diffusion. The effect of molecular diffusion is also restricted. The default values of the turbulent Schmidt number in commercial CFD codes are 0.5–1.5.

2.8. Governing Equations for the Motion of Harmful Dust in CFD

To investigate the motion of dust particles, the force balance equation of particles must be solved [12]. This equation along the x-direction is expressed as

$$\frac{du_p}{dt} = F_D(u - u_p) + \frac{g_x(\rho_p - \rho)}{\rho_p} + F_x$$

where u_p denotes the particle velocity, u denotes the airflow velocity, $F_D(u - u_p)$ denotes the drag force per unit particle mass, and F_x denotes the additional acceleration force per unit particle mass.

Additional details pertaining to this equation can be found in [12]. If the dust particle density is higher, modeling based on the discrete element method (CFD-DEM) is often required to obtain a solution.

2.9. Prediction of the Fluid Age

The age of air is an important factor in mine ventilation. The age of air is defined as the time it takes for air to move from an inlet to a designated point. This quantity is used to determine if the air is fresh. The following equation is used to determine the mean age of air and is employed in commercial CFD codes [13].

$$\frac{\partial}{\partial x_i}\left(\rho u_i - \Gamma\frac{\partial\tau}{\partial x_i}\right) = S_\tau$$

where ρ denotes the density, u denotes the velocity, Γ denotes the diffusion coefficient, τ denotes the mean age of air, and S_τ denotes a source term. The boundary condition at the inlet is zero, whereas that at the outlet and wall is the zero gradient of the mean age of air. Note that this value is strongly influenced by the air velocity.

3. Applications of CFD in Mine Ventilation

In this section, the applications of CFD in mine ventilation are presented as follows. First, the applications of CFD at working or mining faces for the analysis of ventilation of local areas in mines are detailed. Notably, this is a significant application of CFD in mines. Second, the applications of CFD for ventilation of tunnels or galleries in mines are presented. Third, CFD applications in open-pit mines, the design of ventilation systems, and mine thermal energy are introduced. Figure 3 further presents the use of CFD for mine ventilation analysis in the authors' laboratory of this paper. For airflow and gas analysis of entire mines, examples of geometries and grids are presented in Figure 3a. To reduce the proportion of gas and dust, newly built tunnels are tested using CFD. Figure 3b presents the geometries and grids of new fans to be used in mines. Notably, the inclusion of silencers in the fan design is essential for ensuring low noise levels for mine workers. Figure 3c summarizes a parametric study on the optimal locations of two fans near mining faces. Using CFD analysis, both blowing and exhaust fans are optimally located to minimize the amount of dust and harmful gases near mining faces.

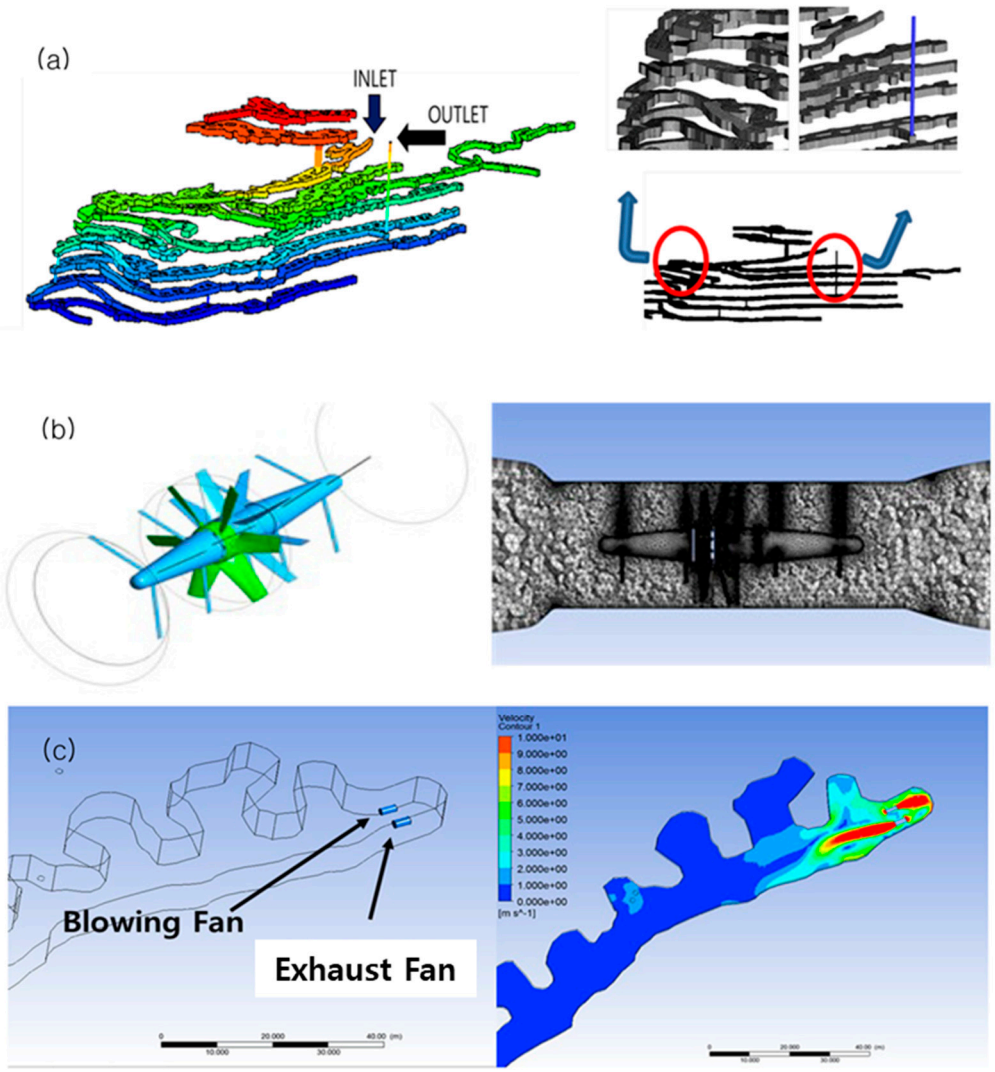

Figure 3. Applications of CFD to mining engineering (**a**) airflow analysis in entire mines (**b**) geometry and grid of a fan used in mine tunnels (**c**) parametric study of optimal locations of two fans near mining faces.

3.1. Ventilation at the Working Faces of Mines

For face ventilation in underground mines, air is locally exhausted or discharged using fans and ducts to decrease the amounts of hazardous gases and dust. So far, various studies have modeled workplaces around mine faces using CFD to analyze hazardous gases and dust. At the faces of mining tunnels, a single blowing duct [14], a single exhaust duct [15], or both [11,15] are used. CFD modeling is primarily based on one or two ducts placed at the working faces.

ANSYS FLUENT, ANSYS CFX, FLOW-3D, and CFD-ACE are typically used to solve the governing equations. FLUENT meshing, ANSYS meshing, ICEM-CFD, and other meshing programs are used to generate grids based on the geometries. The k–ε and SST k–ω models are widely used for turbulence modeling, which implies that both can be employed for initial calculations.

One major advantage of using CFD in mine ventilation studies is that parametric studies at the mining faces can be considered for CFD modeling. The parameters may include blowing ducts or exhaust ducts, discharging and exhaust velocities of the airflow, distance between the blowing or exhaust ducts and the mining face, and location of the blowing and exhaust ducts. These parameters can be optimized using different CFD models.

In their paper, Parra et al. [11] present results on blowing, exhaust, and mixed ventilation, along with a comparison of the experimental and numerical results. For a single blowing duct at the working face, the streamwise velocities are measured using a hot-wire anemometer. The Spalart–Allmaras turbulence model for numerical simulations is used to obtain the velocity distributions. The deviation between the experimental and numerical results is found to be 20%. These experimental results obtained around the mining face serve as the base data for the verification of CFD modeling in other CFD studies.

In another study, Torano et al. [5] compare the data for different turbulence models (i.e., zero equation, k–ε, and Spalart–Allmaras models). They demonstrate that the k–ε model is effective for areas close to the working face, whereas the Spalart–Allmaras model is suitable for application in the developed flow area. The authors use the ANSYS CFX version 10.0 to solve the governing equations, whereas the ICEM-CFD version 10.0 is used to construct the 634k tetra-type grids.

In a different study, Wala et al. [4] conduct base experiments and simulations for CFD code validation using different turbulence models. They use a ventilation test gallery and measure the air velocities and methane concentrations. For CFD calculations, FLUENT 6.X and GAMBIT 2.1 are employed as the solver and grid generator, respectively. Two turbulence models (Spalart–Allmaras and SST k–ω models) are used, and the model with results closer to the experimental values is selected. In that regard, methane distribution results for CFD using the SST k–ω model are found to be close to the experimental results.

Further, Aminossadati et al. [16] present simulations of two-dimensional brattice sails in underground crosscut regions. They obtain velocity data with various brattice lengths. The commercial code, CFD-ACE, and k–ε turbulence model are employed in the calculation. To validate the model, the no-brattice results are compared with those of ANSYS FLUENT; however, no significant difference is observed. A longer brattice is found to lead to enhanced ventilation performance.

In their study, Torano et al. [17] examine the methane concentration near working faces. Here, ANSYS CFX 10.0 is employed to predict methane concentrations, and experimental results are obtained. The k–ε turbulence model is selected for more accurate predictions. Figure 4 depicts the grid generated using ICEM-CFD, along with a comparison between the numerical and experimental results.

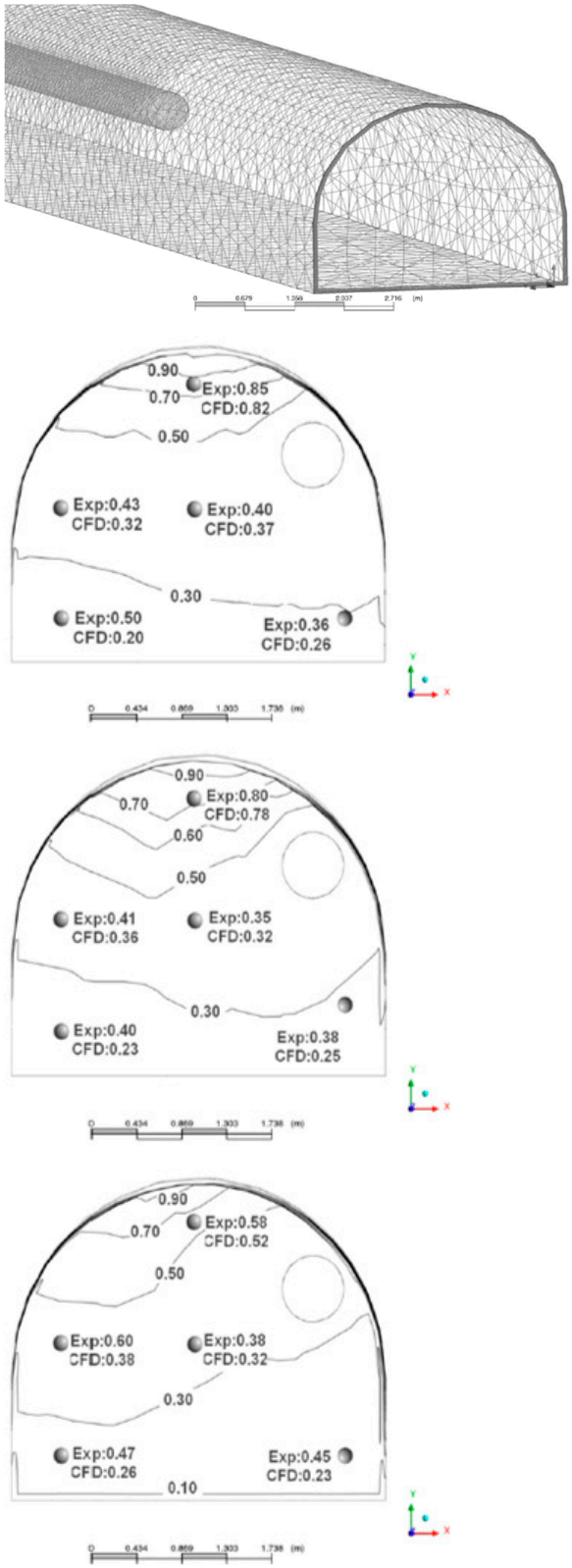

Figure 4. Grid generated for calculation and comparison between the experimental and numerical results (m/s) [17]. (Reprinted with permission from ref. [17]. Copyright 2009 Elsevier B.V.).

In another study, Diego et al. [18] calculate the pressure losses for different roughness values. A comparison between the numerical and theoretical results reveals an error of 17%. ICEM-CFD and ANSYS CFX 10.0 are used to construct meshes and solve different

equations, respectively. The wall function and k–ε model are selected for the calculations. The pressure losses with variations in the wall roughness are predicted using CFD and calculated based on theoretical equations. An error of less than 17% is obtained, which confirms the potential of CFD applications.

Further, Lee [19] presents simulation results obtained based on a parametric study conducted on the working faces of mines. The parameters considered are the duct diameter and duct position. The commercial software ANSYS FLUENT and the realizable k–ε model are employed. The efficiency of air exchange is determined to optimize the position of air ducts.

In a different paper, Torno et al. [20] present numerical results obtained based on an analysis of the blasting gas behavior in working faces. ANSYS CFX 12.0 is employed as the solver, while SolidWorks and ICEM-CFD are used for the geometry and grid generation, respectively. Following the creation of 778 k tetra-calculated grids, the coarse mesh (253 k), fine mesh (1541 k), and intermediate mesh (778 k) are examined based on the grid-independence test. The k–ε turbulence model is selected following comparisons with the Spalart–Allmaras model and SST k–ω model. The simulation results present an unsteady state.

Kurnia et al. [21] further present a new ventilation system at the working faces of mines. They validate their models by comparing their results with the experimental results obtained by Parra et al. [11]. In addition, four turbulence models (Spalart–Allmaras, standard k–ε, standard k–ω, and Reynolds stress models) are tested, and the standard k–ε model is selected. FLUENT 6.3 and Gambit 2.3 are used to obtain the governing equations. Based on a parametric study, an optimal design with reduced methane distribution is obtained from the area-average and volume-average results. In their study, Kurnia et al. [22] simulate the hazardous gas distribution in working faces using shuttle cars, miners, and air ducts. Figure 5a presents schematics of the working area of a mine face with shuttle cars, miners, and blowing ducts. Based on a parametric study, the authors attempt to determine the positions of the tailpipe and duct. Figure 5b illustrates the mass fraction of CO at different planes used to compute the dispersion of gases.

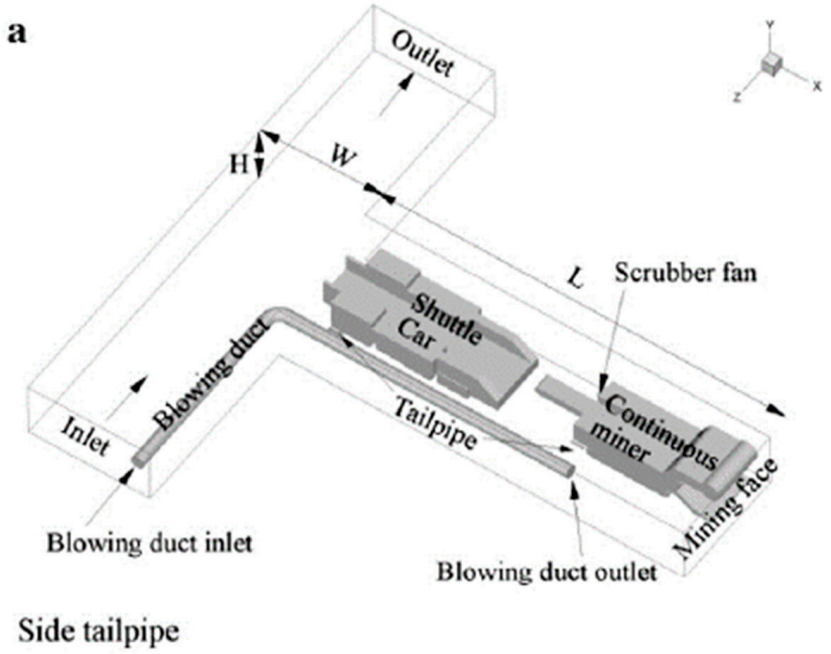

Figure 5. *Cont.*

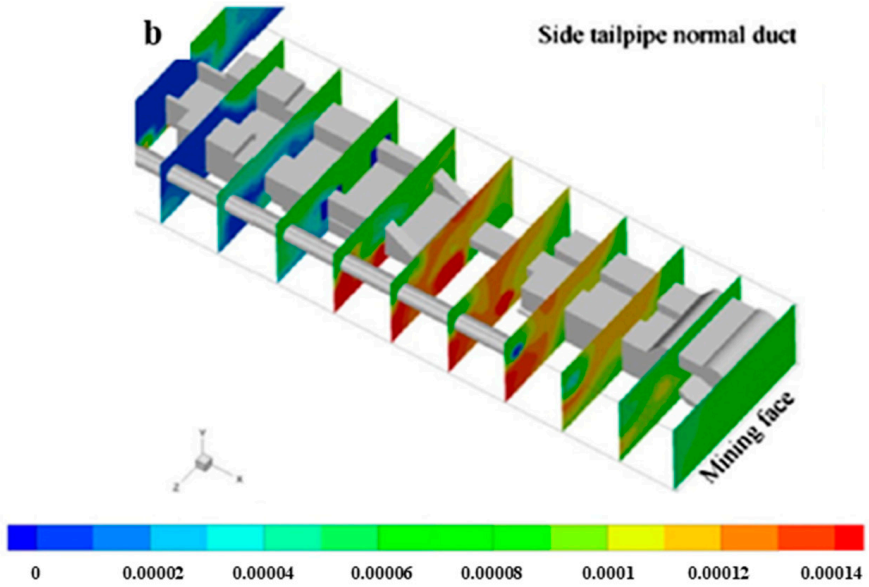

Figure 5. (**a**) Schematics of working area in mine faces with shuttle car, continuous miner, and blowing duct (**b**) mass fraction of nitric dioxide at different planes used to compute dispersion of gases [22]. (Adapted with permission from ref. [22]. Copyright 2014 Elsevier B.V.).

Xu et al. [23] present CFD results for SF_6 dispersion as a tracer gas in mine tunnels. Here, ANSYS FLUENT and ICEM-CFD are used as the solver and the grid generator, respectively. A realizable k–ε model is selected for turbulence modeling. Figure 6a presents a portion of the obtained grids for the cross-section of tunnels composed of both tetra- and hexa-dominated grids. The authors state that hexa-dominated grids present advantages over tetra-dominated grids in terms of solution convergence and grid quality improvement. Figure 6b presents the CFD results of velocity profiles and the SF_6 distribution in the cross-section of mine tunnels. Compared with the experimental results, the velocity errors here are acceptable; however, the CFD results for the SF_6 distribution are approximately 30% lower than the corresponding experimental results. The authors attribute these errors to some differences in the total flow quantity and booster-fan-generated flow quantity compared with the measured and numerical data.

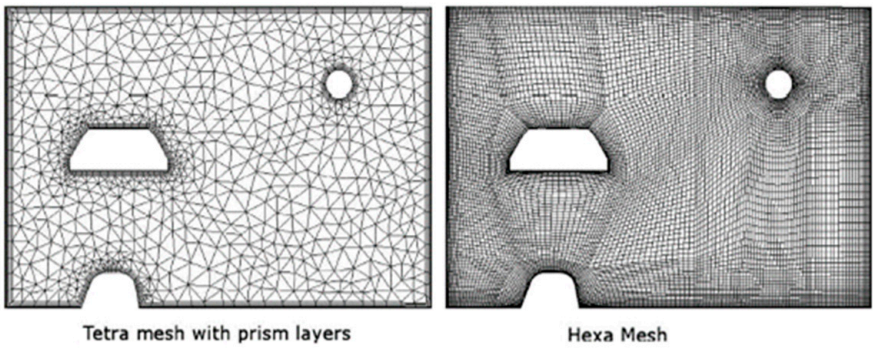

(**a**)

Figure 6. *Cont.*

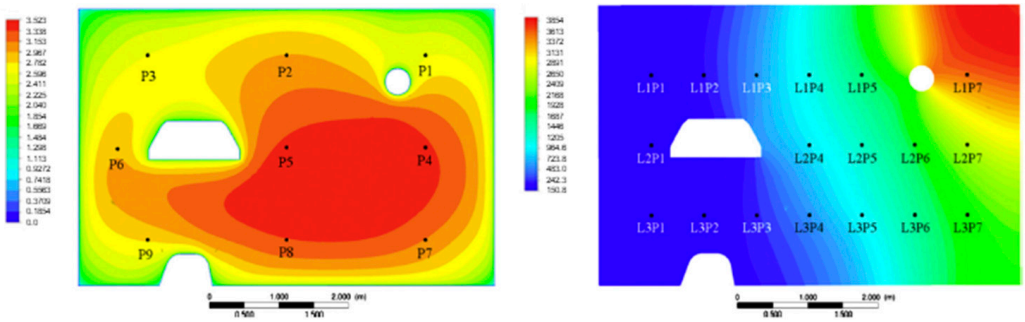

(**b**)

Figure 6. (**a**) a portion of the calculated grids for the cross-section of tunnels made of both tetra- and hexa-dominated grids (**b**) CFD results of the velocity profiles(m/s) and SF_6 distribution(ppb) in the cross-section of mine tunnels [23]. (Adapted with permission from ref. [23]. Copyright 2015 Elsevier Ltd.).

Next, Zhoua et al. [24] simulate methane concentration in the working face of coal mines. For this, ANSYS FLUENT 13.0 is employed to construct the geometry, grids, and as a solver. The standard k–ε model is used to obtain the turbulence. For validation, the CFD results are compared with the measured methane concentration data. Both results appear to be quantitatively similar. A parametric study further indicates that methane release rates affect the methane distribution. Zhoua et al. [25] investigate the methane distribution at the working faces by measuring the air velocities and methane concentrations with varying curtain setback distances. Further, numerical simulations are conducted under the same conditions, and the results are compared with the measurement results. The ANSYS DesignModeler, meshing, and FLUENT 13.0 are employed in this study. A realizable k–ε model is used as the turbulence model. To solve the methane distribution problem, species transport modeling is used. Despite certain differences between the numerical and measured results, the errors appear acceptable.

Zheng et al. [26] investigate the dispersion of diesel particulate matter (DPM) around the dead-end entry of mines. To that end, four cases are studied using the ANSYS FLUENT software. The DPM distributions in mine tunnels with variations in the boundary conditions are presented for four cases.

Li et al. [27] further evaluate the ventilation performance in a working face with large cross-sections. The distributions of CO, dust, air temperature, and oxygen are determined using CFD. Here, ANSYS FLUENT and the standard k–ε model are used as the solver and turbulence model, respectively. Species transport and discrete phase models are employed for gas dispersion and dust dispersion, respectively. The CFD model is validated based on a comparison between the obtained results and the experimental data. The difference between the numerical and experimental results is found to be within an error range of 10%. A value of the minimum air velocity for the ventilation requirements of working faces in mines is obtained.

Lu et al. [28] simulate the dispersion of methane and coal dust in a room-and-pillar mining face. Based on parametric studies considering a fan and the brattice model for CFD, nine cases are considered to identify the optimal operating conditions. Thus, various geometries and operating conditions can be tested using CFD.

In their study, Park et al. [29] investigate the distribution of air velocities, fluid ages, air flow streamlines, and temperatures. For this, ANSYS CFX 16.0 and ICEM-CFD are used as the solver and generator of hexahedral numerical grids, respectively. Figure 7 depicts the obtained geometry, computational grids, and airflow streamlines. A parametric study considering six different duct geometries (cases 1–6) in a working face is conducted to determine the optimal design.

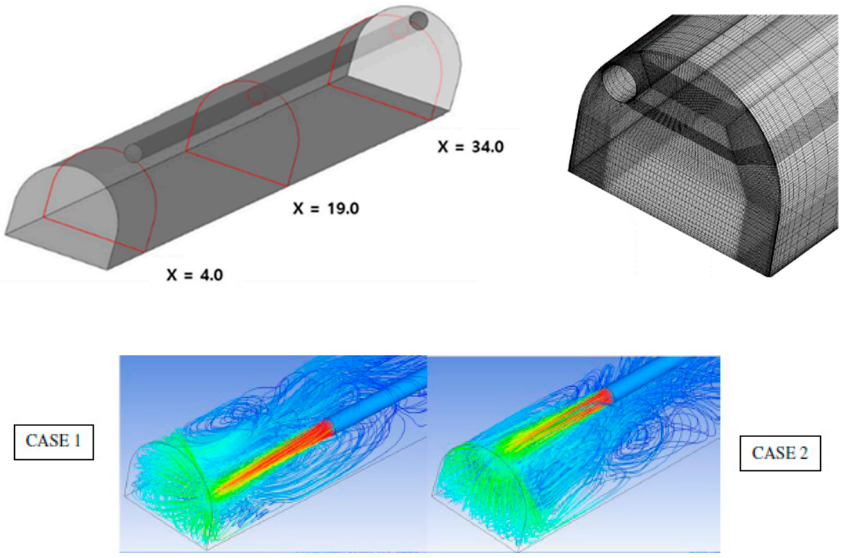

Figure 7. Geometry, computational grid, and airflow streamlines [29]. (Adapted with permission from ref. [29]. Copyright 2016 Taylor & Francis Group).

Coleman et al. [6] propose a dust gallery design based on several ventilation scenarios in underground mines. The Cradle SC/Tetra version 12 software is used as the solver. The geometries for the scenarios are generated using the PTC Creo program. Tetrahedral grids with prism layers are employed to depict near-wall flows. The standard k–ε model is selected as the turbulence model, and six different mining cases are investigated to identify the best configuration for the mines.

Further, Geng et al. [30] examine dust contamination caused by a digging machine at the working faces of mines. The discrete phase model is used to analyze dust behaviors. ANSYS FLUENT and the realizable k–ε model are used for numerical calculations. A structured grid is selected using ICEM-CFD. A comparison between numerical and experimental results reveals good agreement. Parametric studies are also conducted based on the discharge air velocity and exhaust duct length.

In another study, Mishra et al. [31] examine turbulent methane dispersion in the working face of underground coal mines. Herein, ANSYS FLUENT version 12.0 and the standard k–ε model are used as the solver and turbulence model, respectively. Further, parametric studies of the methane distribution are conducted considering the air velocity; methane emission rate; and width, surface roughness, and inclination of the mine gallery.

Park et al. [14] investigate the flow characteristics of a blowing duct installed at the face of underground mines. Here, ANSYS CFX version 17.0, ICEM-CFD, and the k–ε model are used as the solver, grid generator, and turbulence model, respectively. The variations in the following three parameters: distance between the working face and blowing duct, blowing air velocity, and angle of the blowing duct are analyzed to identify optimal design conditions.

Wang et al. [15] investigate airflow characteristics at the longwall face of underground mines. For this, ANSYS FLUENT and the standard k–ε model are used as the solver and turbulence model, respectively. The experimental and numerical results are compared. The air velocities are selected to facilitate comparisons with a marginal error within 10%. Further, parametric studies (parameters: shear position and cutting sequence) are also conducted to determine the optimal locations of blowing ducts.

In their study, Zhang et al. [32] consider dust diffusion in the working faces of mines. Here, ANSYS FLUENT and the standard k–ε model are used as the solver and turbulence model, respectively. A curve-fitting equation between the inlet velocity and dust concentration is presented. Chang et al. [7] evaluate the DPM diffusion in an underground mine based on a CFD parametric study. To that end, three cases related to the length of a blowing duct are analyzed, and the optimal results are presented. Further, a comparison between

the numerical and measured data is provided. The open-source software OpenFOAM and standard k–ε model are used as the solver and turbulence model, respectively.

In their analysis, Wang et al. [15] investigate optimal design values for the thermal environment of a working face. Herein, four designs are evaluated using parameters such as the position, distance, and emitted heat. Finally, an optimal design is obtained using ANSYS FLUENT and the k–ε turbulence model. Liu et al. [33] investigate dust diffusion using an air curtain based on CFD modeling. The variations in the axial-to-radial airflow rate ratio are analyzed, and an optimal design is determined. ANSYS FLUENT and the k–ε turbulence model are employed in the involved analysis.

Kim et al. [10] present the airflow velocity, streamlines, methane concentration, and dust concentration at the working face of underground mines with the installation of one or two ducts. Here, ANSYS CFX version 19.1, ICEM-CFD, and the k–ε turbulence model are used to solve the governing equations. Torno et al. [34] examine the diffusion of toxic fumes in underground mines. The numerical and experimental results for CO and NO_2 diffusion are presented. ANSYS CFX, ICEM-CFD, and the k–ε turbulence model are employed to solve the problems. Moreover, relationship equations between the CFD and experimental values are presented. Yi et al. [35] investigate the airflow characteristics in blowing and exhaust ducts at the mining faces of underground mines. Here, ANSYS CFX, ICEM-CFD, and the k–ε turbulence model are used for the associated calculations. An optimal design is selected based on the fluid age.

In another study, Vives et al. [8] investigate the airflow and temperature in the working face of mines in the presence of one excavator and one dump truck. Four cases, related to the length and angle of the exhaust duct, are considered to identify an optimal design. The FLOW 3D software and k–ε turbulence model are used. Recently, under more complex conditions, CFD has been used to solve the dust dispersion [36–38] and gas problems [39] in mines, including those with large cross-sectional areas [40].

3.2. Mine Ventilation in Mine Tunnels and Galleries

Notably, CFD is suitable for delineating a local area, such as the working face; however, it is also known to provide accurate results for the analysis of a wider area, such as an entire mine gallery or a part of it. Correspondingly, researchers have conducted numerous studies applying CFD to mine galleries and various types of mining structures such as room-and-pillar, block caving, panel cave, and longwall. Moreover, CFD has been used to analyze the movement of airflow in an analysis area, the concentration distribution of dust or toxic gas, and heat transfer. With the progress of research in this field, the considered variables have become optimized, and the dimensional analysis has developed from one-dimensional (1D) to three-dimensional (3D); the analysis is still developing as dimensional fusion analysis. Additionally, with the development of measuring instruments, the complexity of model construction is also expected to evolve.

In their study, Sasmito et al. [41] design a scenario for the installation of various wind screens for gas control in a mine with a room-and-pillar structure; the authors estimate the airflow using CFD. Here, ANSYS FLUENT version 6.3 is used as the solver, and four turbulence models (Spalart–Allmaras, k–ε, k–ω, and Reynolds stress models) are compared to validate CFD models based on the experiments conducted by Parra et al. [11]. Further, the Spalart–Allmaras model is selected owing to its low cost and fast computation.

Erogul et al. [42] examine the relationship between the cave resistance and air-gap height by modeling the vertical cross-section of a mining pool in a block caving mine. For their analysis, the SC/Tetra CFD code and the k–ε turbulence model are used. The parameters considered in the study involve different air velocities with variations in the air-gap heights.

In their study, Juganda et al. [43] present the factors contributing to the airflow and methane accumulation around the walls of longwall mines. The authors suggest that the tailgate of the longwall face represents the primary monitoring point for face ignition. The ANSYS FLUENT software is used as the solver, and two cases (normal tailgate ventilation setup and tailgate entry blocked by roof fall in the longwall face) are analyzed based on CFD modeling.

Baysal et al. [44] derive factors affecting the airflow resistance by simulating a panel cave mine using the CFD code SC/Tetra. Another study develops a mine ventilation simulation method that combines a 3D network model analysis with 1D CFD (Rueda [45]). The foregoing study suggests a method of repeating the 3D analysis by alternately using the Ventsim software and 1D CFD to reset each other's boundary conditions until convergence is achieved. Accordingly, an analysis technique exploiting both the 3D network model and 1D CFD is developed.

In another study, Wang et al. [46] investigate the optimal design of an air curtain device as an alternative refuge in underground mines. For CFD modeling, the RNG k–ε model is used to solve the air flow problem, and a species transport model is used to analyze CO_2 diffusion. The optimal design of the air curtain device is obtained based on parametric studies (mounting angle, baffle, and operating pressure).

Further, Biswal et al. [47] conduct an airflow analysis at various velocities using 3D CFD. Here, CATIA, ANSYS FLUENT, and the standard k–ε model are used as the geometry designer, solver, and turbulence model, respectively. Janus and Krawczyk [48] determine the degree to which the following consideration: "the shape of the model cross-section is constant over the entire length" reduces the accuracy of the simulation results in CFD modeling. Further, boundary conditions are determined using measurement data obtained via a multipoint velocity field measurement system that simultaneously measures the flow velocity at 16 measurement points in the mining face. To accurately represent the shape of the mine gallery, a model closely resembling the actual shape of the mine is obtained using laser scanning technology. The analysis results are compared with the model results based on the assumption. Figure 8 presents a comparison between the numerical and measurement results for three measuring positions.

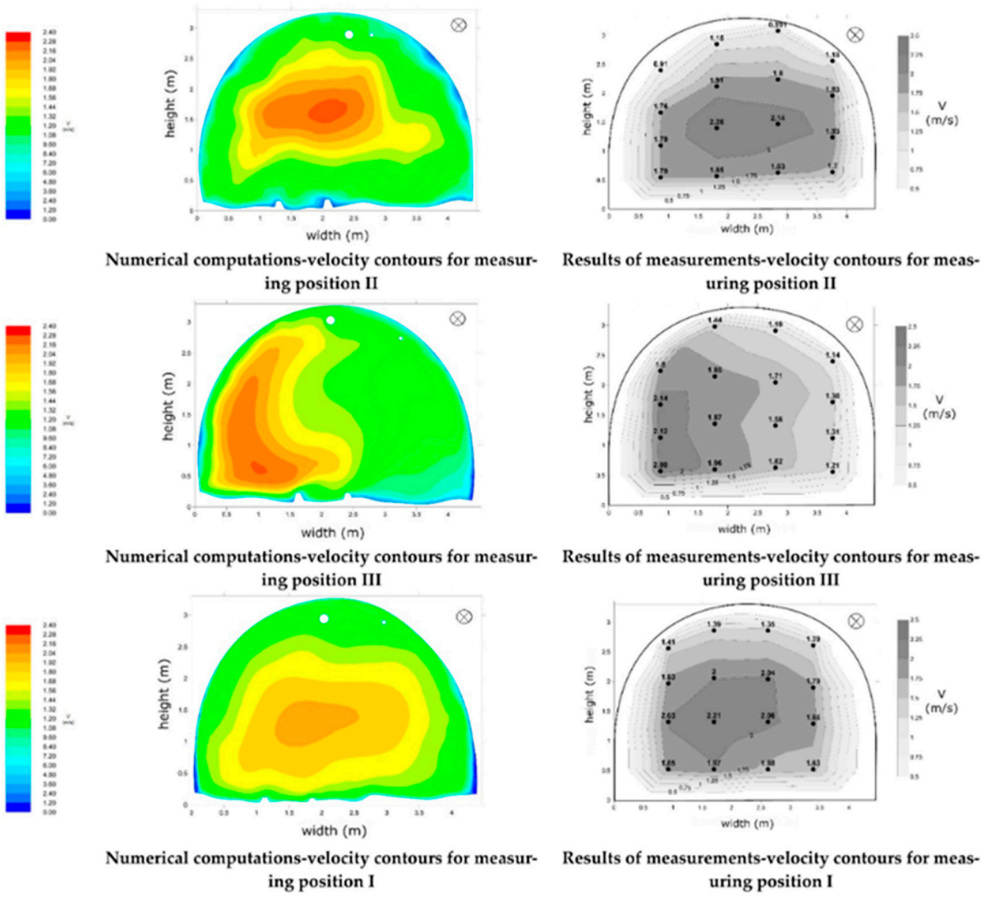

Figure 8. Comparison of the numerical and measurement results (m/s) for three measuring positions [48].

Ajayi et al. [49] simulate the migration of radon gas in block caving mines. The corresponding geometry is designed in three dimensions, and CFD analysis is performed considering the shape of the cross-section. Based on their analysis, the authors identify six parameters affecting the dispersion of toxic gases in the designed model. Further, Lolon et al. [50,51] examine the effects of a barometric pressure drop on the volume and location of explosive gas zones in the gob of a longwall mine. They use CFD to understand the gob outgassing caused by pressure disturbances. In another study, Karacan and Yuan [52] create a fracture network by applying CFD to a longwall gob and simulate the movement and dispersion of toxic gases along the fracture. Kollipara and Chugh [53] further analyze the airflow distribution and dust dispersion in room-and-pillar mines, and Erogul et al. [54] simulate radon contamination in panel cave mines and investigate the changes in airflow resistance based on a geometry with multiple air gaps. Tutak and Brodny [55] apply 3D CFD to analyze the effects of auxiliary ventilation equipment on the methane concentration in coal mines. Saki et al. [56] present a methodology for designing a gob ventilation borehole to control explosive gas zones in a longwall mine using CFD. Further, Wang et al. [57] design an emergency rescue system that is designed to operate in an event of fire in a coal mine. By simulating the temperature and carbon dioxide, oxygen, and carbon monoxide concentrations in the mine, a fire control system based on air volume control is proposed by adjusting the degree of opening of the air door. Further, Balusu et al. [58] establish a strategy to control spontaneous combustion in panel cave mines using CFD. Skob et al. [59] apply CFD to estimate the conditional probability of damage caused to mine personnel and equipment owing to hydrogen explosions. Janoszek et al. [60] investigate aerosol flow based on experimental and numerical methods. The authors provide a quantitative and qualitative prediction of aerosol particle transport.

3.3. CFD Applications in Open-Pit Mines

Raj et al. [61,62] investigate the airflow and pollutant transport in a deep open-pit mine. Here, the LES is selected for turbulence modeling. Using CFD models, various mitigation cases are analyzed to break the air inversion. Further, Bhowmick et al. [63] predict the dust dispersion in a deep open-pit mine. A comparison between the k–ε model and LES results reveals that the latter is better suited for calculating the downfall quantity of dust particles. Kia et al. [64] report the airflow velocities over open-pit mines with variations in the mining depth. The OpenFOAM 4.1 software is used to solve the related equations. Consequently, the effects of the mining depth and thermal stability on flow transport are presented.

3.4. Mine Ventilation Systems

Notably, the design and installation of a ventilation system to improve the air quality inside a mine require careful research and calculations. This can be attributed to the fact that depending on the shape and structure of a mine, the ventilation system may either perform as intended by its designer or aggravate the working environment in the mine. In this respect, combining the design of the mine ventilation system with CFD appears to be an effective approach for realizing the designer's purpose. Depending on the prevailing conditions, several actions such as controlling the airflow speed, changing the airflow direction, separating the space with wind, and collecting dust in the air may be required. To that end, fans, ducts, air curtains, and scrubbers are the primary devices used. Thus far, numerous researchers have simulated the behavior of such devices using CFD.

Haghighat et al. [65] simulate an elbow and louver using ANSYS FLUENT version 14.0 and present the blade angle, elbow angle, cross-sectional shape, and cross-sectional area to minimize leakage and shock losses. Hua et al. [66] compare the ventilation efficiency of the blower and long-compression short-suction methods. Morla and Karekal [67] further present a methodology to optimize the number of fans and their operating positions in a multiseam mine. Here, ANSYS FLUENT version 18 and the standard k–ε model are used to analyze the airflow. In another study, Fernandez [68] conducts 3D CFD analysis to

obtain the change in the velocity path line subject to the fan effect. The author provides suggestions to optimize the geometry of key areas using CFD.

Kurnia et al. [21,69] propose a solution for methane gas management at a mine site by simulating a divider supplying air at a uniform speed and flow rate to the entire mining face. In their analysis, they compare the results of four turbulence models (Spalart–Allmaras, standard k–ε, standard k–ω, and Reynolds stress models) with the experimental results of Parra et al. [11]. Consequently, the k–ε model results are found to demonstrate good agreement with the experimental results, whereas the other model results exhibit only marginal agreement. Further, to reduce the energy consumption of ventilation, the application of intermittent ventilation is analyzed by constructing a relevant scenario.

In their study, Akhtar et al. [70] simulate duct leakage and verify the leakage resistance correlation using ANSYS FLUENT version 16.1 and the k–ε model. They confirm that the influence of pressure varies according to the location and size of the rupture. Guo et al. [71] analyze the dust diffusion law in a tunnel and determine the appropriate air volume in the duct using CFD. Here, ANSYS FLUENT version 16.0 and the discrete phase model are used for dust diffusion.

Further, Arya et al. [72] examine the dust dispersion of a shearer installed with a scrubber in mining tunnels. Based on a CFD parametric study (parameters: scrubber inlet extension, scrubber quantity, and face velocity), dust reduction is analyzed. Consequently, a modified design of the shearer is presented. Obracaj et al. [73] present a duct-and-scrubber overlapping system and verify it based on CFD. Figure 9 presents the numerical results of the velocity streamlines. Here, L_0 is defined as the length of the overlap zones. Four case studies predict the optimal length of the overlap zones. For this, ANSYS FLUENT and the k–ε turbulence model are used, and the performance of the whirl-flow air duct is evaluated. Liu et al. [74] analyze the installation of an air curtain in the face of a coal mine to block dust based on CFD. Yin et al. [75] study the diffusion characteristics of dust contamination according to the location of the air curtain. Here, ANSYS FLUENT, ICEM-CFD, and the realizable k–ε model are used. The airflow and dust distributions for the air curtain generator are presented.

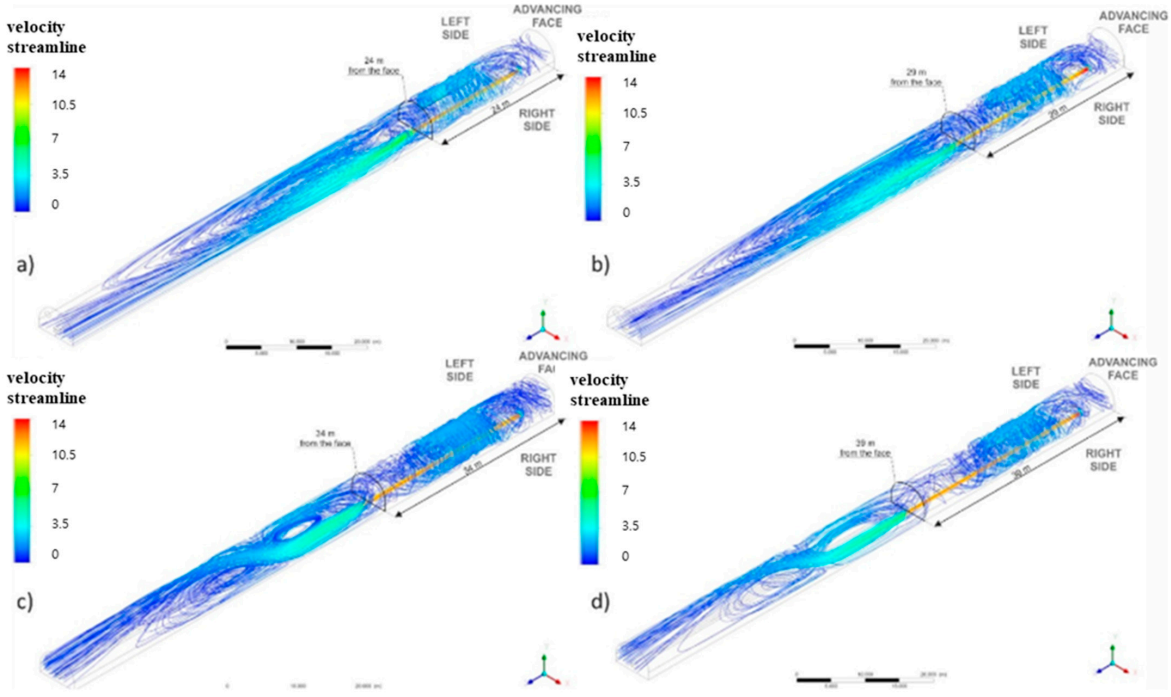

Figure 9. Numerical results of the velocity streamlines (**a**) L_0 = 5m, (**b**) L_0 = 10m, (**c**) L_0 = 15m, (**d**) L_0 = 20m [73].

Hua et al. [76,77] further simulate the dust reduction effect according to the air volume of an air curtain, present a 3D spiral wind-curtain, and test its effect. Figure 10 presents a schematic of the velocity distribution in the 3D spiral wind-curtain. The performance of the multiradial vortex airflow generator is tested using ANSYS FLUENT 16.0.

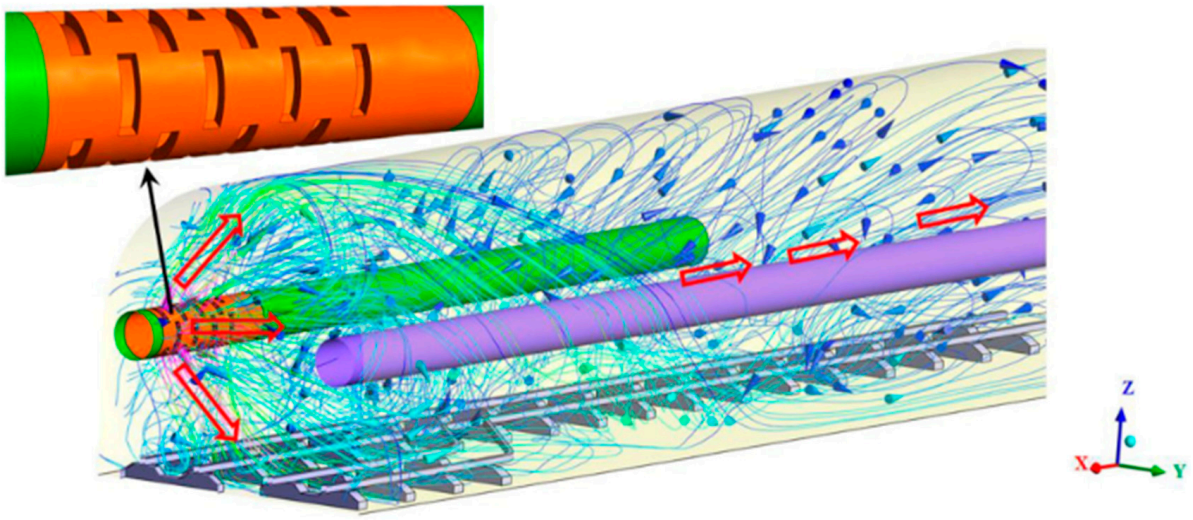

Figure 10. A schematic diagram of the velocity streamlines of the 3D spiral wind-curtain [76]. (Adapted with permission from ref. [76]. Copyright 2020 Elsevier Ltd.).

Wedding et al. [78] present the conceptual design of a scrubber for dust collection in underground coal mines. Since their study, several researchers have developed various scrubber prototypes and dust sensors and analyzed their performance using CFD (Geortz et al. [79]; Kumar et al. [80]; Zhou et al. [81]; Arya et al. [82]). Chen et al. [83] devise a new dust removal system and simulate a wet dust collection net using CFD. Further, Xiu et al. [84] derive the appropriate level of ventilation flow for optimal dust collection. Hua et al. [77] develop a multiradial vortex-based ventilation system and simulate it using CFD. Moreover, optimal designing of two-fan parallel stations [85] and small air-cooling towers [86] has been recently conducted for mine ventilation.

3.5. CFD Applications for Mine Fire and Thermal Energy

Typically, mine fires produce hazardous gases, heat, and dust. Several types of fires, including methane explosions, diesel truck fires, and conveyor belt fires, can occur in mines. Furthermore, deep mining involves working in high-temperature zones, and experimentally analyzing fires and thermal flows is often challenging. However, CFD can easily and accurately predict the diffusion of fire and heat in mines.

Adjiski [87] investigates the smoke rollback effect in underground mines. Notably, fire rollback occurs when combustion products, such as smoke and gas, flow in the opposite direction of the primary ventilation flow. In the foregoing analysis, the PyroSim software is used for the fire dynamics simulation, and the LES model is used as the turbulence model.

Lee et al. [88] investigate the characteristics of a diesel engine fire in large limestone mines. The diffusion of smoke and heat is analyzed based on the commercial CFD software SOLVENT version 1.0. Based on the simulation of two scenarios, the fire behavior and risk of back-layering and choking effects are observed.

Yuan et al. [89] examine the characteristics of a water spray during a conveyor belt fire at a mine entry using the CFD software NIST Fire Dynamics Simulator version 5. The related parametric study considers the water droplet size, initial velocity, and spray angles. The corresponding results indicate that to reduce the downstream smoke temperature, the water droplet size is a more critical factor than the initial velocity and spray angle.

Zhou et al. [90] examine the cooling effects of a ventilation duct in high-temperature mines. The CFD software ANSYS FLUENT, ICEM-CFD, k–ε model are used as the solver,

grid generator, and turbulence model, respectively. Accordingly, six models are analyzed, and single and double tubes are considered as the main parameters. An optimal design is identified to reduce the temperature in the tunnel.

Huang et al. [91] investigate the freezing of roadways in high altitude mines using ANSYS FLUENT and the k–ε turbulence model. The calculation parameters include the altitude, inlet airflow volume, and temperature difference. The authors suggest that the convective temperature difference is the most significant factor affecting heat loss.

Xin et al. [92] investigate the thermal performance of force and exhaust ducts in the working faces of underground mines using ANSYS FLUENT as the solver and the standard k–ε model as the turbulence model. The cooling performance is analyzed in four basic cases, and an optimal design is determined based on a parametric study. Using CFD case studies, mine fire behavior is evaluated under different operating conditions [93,94], and a fire dynamics simulator is employed for the calculations.

Table 1 presents a comparison between various CFD applications in the analysis of mine ventilation. Parra et al. [11] conduct base experiments, and the results obtained are beneficial for the validation of models developed in existing studies [14,22]. Based on their research, many papers can be established that study geometries for the ventilation systems of mining faces which are primarily focused on the design of blowing and exhaust ducts, and the Spalart–Allmaras or the k–ε model is primarily selected as the turbulence model. The results of the involved investigations present airflow velocities, dust concentration, gas (such as SF_6, CO, NO_2, and CH_4) concentration, and temperature distribution in mine ventilation systems. Xu et al. [23] present the SF_6 distribution and a comparison of experimental and numerical results. These experiments are critical because they indicate that the gas concentration can be used in the modeling validation of CFD results.

Table 1. Comparison between CFD applications in mine ventilation systems.

References	Base Experiment for Validation	Problems	Turbulence Model	Solver	Parameters or Results
Parra et al. [11]	Experiment conducted by the authors	Blowing and exhaust duct at the mining face	Spalart–Allmaras	Not mentioned	Location and length of ducts
Torano et al. [5]	Experiment conducted by the authors	Blowing duct at the mining face	k–ε	CFX 10.0	Calculated cross-section
Wala et al. [4]	Experiment conducted by the authors	Blowing curtain at mining face	SST k–ω	FLUENT	Airflow and methane distribution
Kurnia et al. [22]	Parra et al. [11]	New blowing duct at the mining face	k–ε	FLUENT 6.3	Inlet velocity and various geometries of ducts
Xu et al. [23]	Experiment conducted by the authors	SF_6 concentration in tunnels	k–ε	ANSYS FLUENT	SF_6 concentration with time
Zhou et al. [25]	Experiment conducted by the authors	Gas concentration	k–ε	ANSYS FLUENT 13	Gas concentration with blowing curtains
Park et al. [14]	Parra et al. [11]	Blowing duct at the mining face	k–ε	ANSYS CFX 17	Locations of ducts and airflow velocity
Torno et al. [34]	Experiment conducted by the authors	CO and NO_2 diffusion at the mining face	k–ε	ANSYS CFX	CO and NO_2 distribution with time
Vives et al. [8]	Experiment conducted by the authors	Optimal location of a blowing duct	k–ε	FLOW-3D	Temperature distribution with various duct positions
Obracaj et al. [73]	Experiment conducted by the authors	Methane distribution with blowing and exhaust ducts	k–ε	ANSYS FLUENT 2020	Methane distribution with a whirl-flow air duct
Xin et al. [92]	Experiment conducted by the authors	Four cases of both blowing and exhaust ducts	k–ε	ANSYS FLUENT	Temperature and airflow distribution with various positions of ducts

4. Summary and Conclusions

Herein, to provide an overview of CFD applications in mine ventilation analysis, studies on the working faces and tunnels in underground mines and open-pit mines published since the year 2000 are reviewed. In addition, the results of CFD modeling aimed at the design of fans and ducts and the determination of thermal energy are presented.

Detailed CFD modeling procedures are introduced to obtain building geometries, generate grids, and solve the governing equations. Based on our review, the applications of the CFD model in the working faces and tunnels appear to be partially focused on the optimal design of blowing and exhaust ducts, and novel designs for ducts with improved performance are introduced. Moreover, airflows and gas and dust dispersions are also analyzed in numerous studies. Consequently, new designs for fans and ducts are considered to decrease the amounts of hazardous gas and harmful dust in underground mines.

Thus, CFD is an excellent tool for investigating airflows and gas and dust dispersion in underground mines. However, several differences between the CFD results and experimental results still remain. These differences can primarily be attributed to the roughness of mine walls, difficulties in the precise simulations of mining environments, problems in the grid quality, and issues in the selection of turbulence models. Particularly, rough surfaces create complicated turbulent flows, thereby complicating the simulation of airflows within mines. Thus, if the surface wall in the investigated area of mines is particularly rough, the effect of roughness should be necessarily considered. Furthermore, exact data on the airflow properties (velocity, pressure, temperature, and humidity) in mine fields should be obtained and used for CFD models. Only when the error between the CFD and experimental results is minimized, the performance of CFD in analyzing and modeling mine ventilation will improve.

In future, we believe that CFD may be beneficial in realizing digital mines. However, for this, the applications of CFD to entire mines, as well as to local areas, should be investigated. Although a large number of grids will require more computing time, we believe that advances in computing technology will make this task achievable. Furthermore, additional and comprehensive experimental data are needed for improved CFD-based modeling of mines.

Author Contributions: Conceptualization, H.Y. and J.P.; reviewing and writing—first draft, H.Y., M.K., D.L. and J.P.; writing-final version, H.Y. and J.P.; project administration, J.P.; funding acquisition, J.P. All authors have read and agreed to the published version of the manuscript.

Funding: This study was supported by the Korea Institute of Geoscience and Mineral Resources (KIGAM) Research Project "Development of precise exploration technology for energy storage minerals (V) existing in Korea and the resources estimation" funded by the Ministry of Science and ICT of Korea.

Conflicts of Interest: The authors declare no conflict of interest.

References

1. Anderson, J.D. *Computational Fluid Dynamics*; McGraw-Hill: New York, NY, USA, 1995.
2. Versteeg, H.K.; Malalasekera, W. *An Introduction to Computational Fluid Dynamics*, 2nd ed.; Prentice Hall, Pearson Education Ltd.: London, UK, 2007.
3. Patankar, S.V. *Numerical Heat Transfer and Fluid Flow*; Hemisphere Publishing Corporation: New York, NY, USA, 1980.
4. Wala, A.M.; Vytla, S.; Taylor, C.D.; Huang, G. Mine face ventilation: A comparison of CFD results against benchmark experiments for the CFD code validation. *NIOSH Min. Eng.* **2007**, *59*, 49–55.
5. Torano, J.; Rodriguez, R.; Diego, I. Computational Fluid Dynamics (CFD) use in the simulation of the death end ventilation in tunnels and galleries. *WIT Trans. Eng. Sci.* **2006**, *52*, 113–121.
6. Coleman, B.; Wedding, W.C.; Petrov, T. Design considerations for construction of a face ventilation gallery using computational fluid dynamics modeling. In Proceedings of the 16th North American Mine Ventilation Symposium, Golden, CO, USA, 17–22 July 2017.
7. Chang, P.; Xu, G.; Zhou, F.; Mullins, B.; Abishek, S.; Chalmers, D. Minimizing DPM pollution in an underground mine by optimizing auxiliary ventilation systems using CFD. *Tunn. Undergr. Space Technol.* **2019**, *87*, 112–121. [CrossRef]

8. Vives, J.; Bascompta, M.; Felipe, J.J.; Sanmiquel, L. Computational Fluid Dynamics (CFD) study to optimize the auxiliary ventilation system in an underground mine. *DYNA* **2022**, *89*, 84–91. [CrossRef]
9. Menter, F. Two-equation Eddy-viscosity Turbulence Model for Engineering Applications. *AIAA J.* **1994**, *32*, 1598–1605. [CrossRef]
10. Kim, M.; Park, J.; Jo, Y.; Lee, D.; Yi, H. Numerical Investigation of Characteristics of Mine Ventilation Using One or Two Ducts in Underground Mining Faces. In Proceedings of the International Conference on Innovations for Sustainable and Responsible Mining, Hanoi, Vietnam, 15–17 October 2020.
11. Parra, M.T.; Villafruela, J.M.; Castro, F.; Mendez, C. Numerical and experimental analysis of different ventilation systems in deep mines. *Build. Environ.* **2006**, *41*, 87–93. [CrossRef]
12. ANSYS. *ANSYS FLUENT Theory Guide*; ANSYS: Canonsburg, PA, USA, 2016.
13. Sun, D. *Computational Fluid Dynamics in Food Processing*; CRC-Press: Boca Raton, FL, USA, 2007.
14. Park, J.; Jo, Y.; Park, G. Flow characteristics of fresh air discharged from a ventilation duct for mine ventilation. *J. Mech. Sci. Technol.* **2018**, *32*, 1187–1194. [CrossRef]
15. Wang, W.; Zhang, C.; Yang, W.; Xu, H.; Li, S.; Li, C.; Ma, H.; Qi, G. In Situ Measurements and CFD Numerical Simulations of Thermal Environment in Blind Headings of Underground Mines. *Processes* **2019**, *7*, 313. [CrossRef]
16. Aminossadati, S.M.; Hooman, K. Numerical Simulation of Ventilation Air Flow in Underground Mine Workings. In Proceedings of the 12th U.S./North American Mine Ventilation Symposium, Reno, NV, USA, 9–11 June 2008.
17. Torano, J.; Torno, S.; Menendez, M.; Gent, M.; Velasco, J. Models of methane behavior in auxiliary ventilation of underground coal mining. *Int. J. Coal Geol.* **2009**, *80*, 35–43. [CrossRef]
18. Diego, I.; Torno, S.; Torano, J.; Menendez, M.; Gent, M. A practical use of CFD for ventilation of underground works. *Tunn. Undergr. Space Technol.* **2011**, *26*, 189–200. [CrossRef]
19. Lee, D.K. A Computational Flow Analysis for Choosing the Diameter and Position of an Air Duct in a Working Face. *J. Min. Sci.* **2011**, *47*, 664–674. [CrossRef]
20. Torno, S.; Torano, J.; Ulecia, M.; Allende, C. Conventional and numerical models of blasting gas behaviour in auxiliary ventilation of mining headings. *Tunn. Undergr. Space Technol.* **2013**, *34*, 73–81. [CrossRef]
21. Kurnia, J.C.; Sasmito, A.P.; Mujumdar, A.S. Simulation of a novel intermittent ventilation system for underground mines. *Tunn. Undergr. Space Technol.* **2014**, *42*, 206–215. [CrossRef]
22. Kurnia, J.C.; Sasmito, A.P.; Wong, W.Y.; Mujumdar, A.S. Prediction and innovative control strategies for oxygen and hazardous gases from diesel emission in underground mines. *Sci. Total Environ.* **2014**, *481*, 317–334. [CrossRef] [PubMed]
23. Xu, G.; Jong, E.C.; Luxbacher, K.D.; Ragab, S.A.; Karmis, M.E. Remote characterization of ventilation systems using tracer gas and CFD in an underground mine. *Saf. Sci.* **2015**, *74*, 140–149. [CrossRef]
24. Zhoua, L.; Pritchardb, C.; Zhenga, Y. Computational fluid dynamics modeling of methane distribution at a continuous miner face under various methane release conditions. In Proceedings of the 15th U.S./North American Mine Ventilation Symposium, Blacksburg, VA, USA, 21–25 June 2015; pp. 419–426.
25. Zhoua, L.; Pritchardb, C.; Zhenga, Y. CFD modeling of methane distribution at a continuous miner face with various curtain setback distances. *Int. J. Min. Sci. Technol.* **2015**, *25*, 297–306. [CrossRef]
26. Zheng, Y.; Thiruvengadam, M.; Lan, H.; Tien, J.C. Simulation of DPM Dispersion for Different Mining Operations Inside a Dead-end Entry. In Proceedings of the 15th U.S./North American Mine Ventilation Symposium, Blacksburg, VA, USA, 21–25 June 2015; pp. 297–306.
27. Li, M.; Aminossadati, S.M.; Wu, C. Numerical simulation of air ventilation in super-large underground developments. *Tunn. Undergr. Space Technol.* **2016**, *52*, 38–43. [CrossRef]
28. Lu, Y.; Akhtar, S.; Sasmito, A.P.; Kurnia, J.C. Numerical Study of simultaneous methane and coal dust dispersion in a room and pillar mining face. In Proceedings of the 3rd International Symposium on Mine Safety Science and Engineering, Montreal, QC, Canada, 13–19 August 2016.
29. Park, J.; Park, S.; Lee, D. CFD modeling of ventilation ducts for improvement of air quality in closed mines. *Geosyst. Eng.* **2016**, *19*, 177–187. [CrossRef]
30. Geng, F.; Luo, G.; Wang, Y.; Peng, Z.; Hu, S.; Zhang, T.; Chai, H. Dust dispersion in a coal roadway driven by ahybrid ventilation system: A numerical study. *Process Saf. Environ. Prot.* **2018**, *113*, 388–400. [CrossRef]
31. Mishra, D.P.; Panigrahi, D.C.; Kumar, P. Computational investigation on effects of geo-mining parameters on layering and dispersion of methane in underground coal mines- A case study of Moonidih Colliery. *J. Nat. Gas Sci. Eng.* **2018**, *53*, 110–124. [CrossRef]
32. Zhang, Q.; Zhou, G.; Qian, X.; Yuan, M.; Sun, Y.; Wang, D. Diffuse pollution characteristics of respirable dust in fully-mechanized mining face under various velocities based on CFD investigation. *J. Clean. Prod.* **2018**, *184*, 239–250. [CrossRef]
33. Liu, Q.; Nie, W.; Hua, Y.; Peng, H.; Liu, C.; Wei, C. Research on tunnel ventilation systems: Dust Diffusion and Pollution Behaviour by air curtains based on CFD technology and field measurement. *Build. Environ.* **2019**, *147*, 444–460. [CrossRef]
34. Torno, S.; Torano, J. On the prediction of toxic fumes from underground blasting operations and dilution ventilation. Conventional and numerical models. *Tunn. Undergr. Space Technol.* **2020**, *96*, 103194. [CrossRef]
35. Yi, H.; Park, J.; Kim, M. Characteristics of mine ventilation air flow using both blowing and exhaust ducts at the mining face. *J. Mech. Sci. Technol.* **2020**, *34*, 1167–1174. [CrossRef]

36. Jiang, W.; Xu, X.; Wen, Z.; Wei, L. Applying the similarity theory to model dust dispersion duringcoal-mine tunneling. *Process Saf. Environ. Prot.* **2021**, *148*, 415–442. [CrossRef]
37. Duan, J.; Zhou, G.; Yang, Y.; Jing, B.; Hu, S. CFD numerical simulation on diffusion and distribution of diesel exhaust particulates in coal mine heading face. *Adv. Powder Technol.* **2021**, *32*, 3660–3671. [CrossRef]
38. Zhou, G.; Jing, B.; Xu, Z.; Jiang, B.; Xu, R.; Ren, B.; Sun, B. Simulation study on gas-bearing dust and its application combined with air curtain in development heading, a case study. *Process Saf. Environ. Prot.* **2022**, *163*, 601–612. [CrossRef]
39. Rahimi, S.; Ataee-pour, M.; Madani, H.; Aminossadati, S.M. Investigating the impact of gas emission uncertainty on airflow distribution in an auxiliary ventilation system using CFD and Monte-Carlo simulation. *Build. Environ.* **2021**, *204*, 108165. [CrossRef]
40. Du, T.; Nie, W.; Chen, D.; Xiu, Z.; Yang, B.; Liu, Q. CFD modeling of coal dust migration in an 8.8-meter-high fully mechanized mining face. *Energy* **2020**, *212*, 118616. [CrossRef]
41. Sasmito, A.P.; Birgersson, E.; Ly, H.C.; Mujumdar, A.S. Some approaches to improve ventilation system in underground coal mines environment—A computational fluid dynamic study. *Tunn. Undergr. Space Technol.* **2013**, *34*, 82–95. [CrossRef]
42. Erogul, D.; Baysal, A.; Ajayi, K.M.; Tukkaraja, P.; Shahbazi, K.; Katzenstein, K.; Loring, D. Effect of the Air Gap Associated with Cave Evolution on Cave Resistance. In Proceedings of the 15th North American Mine Ventilation Symposium, Blacksburg, VA, USA, 21–25 June 2015.
43. Juganda, A.; Brune, J.F.; Bogin Jr, G.E.; Grubb, J.W.; Lolon, S.A. CFD Modeling of Longwall Tailgate Ventilation Conditions. In Proceedings of the 16th North American Mine Ventilation Symposium, Golden, CO, USA, 17–22 July 2017.
44. Baysal, A.; Ajayi, K.M.; Tukkaraja, P.; Shahbazi, K.; Katzenstein, K.; Loring, D. Prediction of Airflow Resistance of a Mature Panel Cave. In Proceedings of the 16th North American Mine Ventilation Symposium, Golden, CO, USA, 17–22 July 2017.
45. Rueda, N. Co-simulation: 1D to 3D coupling in an underground mine ventilation simulated model. In Proceedings of the 16th North American Mine Ventilation Symposium, Golden, CO, USA, 17–22 July 2017.
46. Wang, Z.; Ren, T.; Ma, L.; Zhang, J. Investigations of Ventilation Airflow Characteristics on a Longwall Face—A Computational Approach. *Energies* **2017**, *11*, 1564. [CrossRef]
47. Biswal, P.K.; Parida, D.; Mishra, G.; Sahoo, A.K. Study of air flow pattern in mine model gallery and its validation using CFD modelling. *WSN* **2019**, *130*, 1–24.
48. Janus, J.; Krawczyk, J. Measurement and Simulation of Flow in a Section of a Mine Gallery. *Energies* **2021**, *14*, 4894. [CrossRef]
49. Ajayi, K.M.; Tukkaraja, P.; Shahbazi, K.; Katzenstein, K.; Loring, D. Computational Fluid Dynamics Study of Radon Gas Migration in a Block Caving Mine. In Proceedings of the 15th North American Mine Ventilation Symposium, Blacksburg, VA, USA, 21–25 June 2015.
50. Lolon, S.A.; Gilmore, R.C.; Brune, J.F.; Bogin Jr, G.E.; Grubb, J.W.; Zipf Jr, R.K.; Juganda, A.; Saki, S.A. Effect of Decreasing Barometric Pressure on Explosive Gas Zones in Bleeder Ventilated Longwall Gobs. In Proceedings of the 15th North American Mine Ventilation Symposium, Blacksburg, VA, USA, 21–25 June 2015.
51. Lolon, S.; Brune, J.F.; Bogin Jr, G.E.; Grubb, J.W.; Juganda, A. Understanding Gob Outgassing Associated with Pressure Disturbances in Longwall Mine. In Proceedings of the 16th North American Mine Ventilation Symposium, Golden, CO, USA, 17–22 July 2017.
52. Karacan, C.O.; Yuan, L. Effect of Discrete Fracture Network Representation of Gob on Airflow Distribution Near the Longwall Face. In Proceedings of the 15th North American Mine Ventilation Symposium, Blacksburg, VA, USA, 21–25 June 2015.
53. Kollipara, V.K.; Chugh, Y.P. CFD Modeling of Dust Dispersion in a Room-and-Pillar Mining Area: A Case Study. *Int. J. Environ. Poll.* **2016**, *59*, 230–249.
54. Erogul, D.; Ajayi, K.M.; Tukkaraja, P.; Shahbazi, K.; Katzenstein, K.; Loring, D. Evaluation of Cave Airflow Resistance Associated with Multiple Air Gap Geometries during Cave Evolution. In Proceedings of the 16th North American Mine Ventilation Symposium, Golden, CO, USA, 17–22 July 2017.
55. Tutak, M.; Brodny, J. Analysis of the Impact of Auxiliary Ventilation Equipment on the Distribution and Concentration of Methane in the Tailgate. *Energies* **2018**, *11*, 3076. [CrossRef]
56. Saki, S.A.; Brune, J.F.; Khan, M.U. Optimization of gob ventilation boreholes design in longwall mining. *Int. J. Min. Sci. Techol.* **2020**, *30*, 811–817. [CrossRef]
57. Wang, K.; Jiang, S.; Ma, X.; Wu, Z.; Shao, H.; Zhang, W.; Cui, C. Numerical simulation and application study on a remote emergency rescue system during a belt fire in coal mines. *Nat. Hazards* **2016**, *84*, 1463–1485. [CrossRef]
58. Balusu, R.; Belle, B.; Tanguturi, K. Development of gas and spontaneous combustion control strategies for 6.0 km long longwall panels. In Proceedings of the 16th North American Mine Ventilation Symposium, Golden, CO, USA, 17–22 July 2017.
59. Skob, Y.A.; Ugryumov, M.L.; Granovskiy, E.A. Numerical assessment of hydrogen explosion consequences in a mine tunnel. *Int. J. Hydrog. Energy* **2021**, *46*, 12361–12371. [CrossRef]
60. Janoszek, T.; Lubosik, Z.; Swierczek, L.; Walentek, A.; Jaroszewicz, J. Experimental and CFD Simulations of the Aerosol Flow in the Air Ventilating the Underground Excavation in Terms of SARS-CoV-2 Transmission. *Energies* **2021**, *14*, 4743. [CrossRef]
61. Raj, K.V.; Bandopadhyay, S. A Large Eddy Simulation Model of Air Flow and Pollutant Transport in a Deep Open Pit Mine under Arctic Inversion. In Proceedings of the SME Annual Meeting, Salt Lake City, UT, USA, 23–26 February 2014.
62. Raj, K.V.; Bandopadhyay, S. Mitigation of Pollutants in Deep Open-Pit Mines under Arctic Air Inversion. In Proceedings of the 16th North American Mine Ventilation Symposium, Golden, CO, USA, 17–22 July 2017.

63. Bhowmick, T.; Bandopadhyay, S. Comparison of Turbulence Models for Estimation of Fugitive Dust Retention in Open-Pit Mines. In Proceedings of the 15th North American Mine Ventilation Symposium, Blacksburg, VA, USA, 21–25 June 2015.
64. Kia, S.; Flesch, T.K.; Freeman, B.S.; Aliabadi, A.A. Atmospheric transport over open-pit mines: The effects of thermal stability and mine depth. *J. Wind Eng. Ind. Aerodyn.* **2021**, *214*, 104677. [CrossRef]
65. Haghighat, A.; Gillies, S.; Luxbacher, K. Behavior of Flow through Mine Elbows and Louvers. In Proceedings of the 15th North American Mine Ventilation Symposium, Blacksburg, VA, USA, 21–25 June 2015.
66. Hua, Y.; Nie, W.; Cai, P.; Liu, Y.; Peng, H.; Liu, Q. Pattern characterization concerning spatial and temporal evolution of dust pollution associated with two typical ventilation methods at fully mechanized excavation faces in rock tunnels. *Powder Techol.* **2018**, *334*, 117–131. [CrossRef]
67. Morla, R.; Karekal, S. Selection of fan(s) to dilute DPM for multi-seam board and pillar coal mines using Hardy Cross and CPM methods. *Int. J. Eng. Technol. Manag.* **2018**, *6*, 36–47.
68. Fernandez, J. Using ventilation to drive mine productivity. In Proceedings of the the Australian Mine Ventilation Conference, Perth, Australia, 26–28 August 2019.
69. Kurnia, J.C.; Sasmito, A.P.; Mujundar, A.S. CFD simulation of methane dispersion and innovative methane management in underground mining faces. *Appl. Math Model.* **2014**, *38*, 3467–3484. [CrossRef]
70. Akhtar, S.; Kumral, F.M.; Sasmito, A.P. Evaluation of duct leakage estimation methods in an auxiliary mine ventilation system: Empirical vs computational fluid dynamics. In Proceedings of the 16th North American Mine Ventilation Symposium, Golden, CO, USA, 17–22 July 2017.
71. Guo, L.; Nie, W.; Yin, S.; Liu, Q.; Hua, Y.; Cheng, L.; Cai, X.; Xiu, Z.; Du, T. The dust diffusion modeling and determination of optimal airflow rate for removing the dust generated during mine tunneling. *Build Env.* **2020**, *178*, 106846. [CrossRef]
72. Arya, S.; Sottile, J.; Novak, T. Numerical Modeling of a Flooded-Bed Dust Scrubber Integrated into a Longwall Shearer. *Min. Metall. Explor.* **2020**, *37*, 1105–1119. [CrossRef]
73. Obracaj, D.; Karzec, M.; Deszcz, P. Study onMethane Distribution in the Face Zone of the Fully Mechanized Roadway with Overlap Auxiliary Ventilation System. *Energies* **2021**, *14*, 6379. [CrossRef]
74. Liu, Q.; Nie, W.; Hua, Y.; Peng, H.; Liu, Z. The effects of the installation position of a multi-radial swirling air-curtain generator on dust diffusion and pollution rules in a fully-mechanized excavation face: A case study. *Powder Technol.* **2018**, *329*, 371–385. [CrossRef]
75. Yin, S.; Nie, W.; Liu, Q.; Hua, Y. Transient CFD modelling of space-time evolution of dust pollutants and air-curtain generator position during tunneling. *J. Clean. Prod.* **2019**, *239*, 117924. [CrossRef]
76. Hua, Y.; Nie, W.; Liu, Q.; Yin, S.; Peng, H. Effect of wind curtain on dust extraction in rock tunnel working face: CFD and field measurement analysis. *Energy* **2020**, *197*, 117214. [CrossRef]
77. Hua, Y.; Nie, W.; Guo, L.; Cai, X.; Cheng, L. The control effect of 3D spiral wind-curtain generator on respirable dust pollution during tunnelling process. *Environ. Sci. Pollut. Res.* **2021**, *28*, 68212–68228. [CrossRef]
78. Wedding, W.C.; Novak, T.; Arya, S.; Kumar, A. CFD Modeling of a Flooded-Bed Scrubber Concept for a Longwall Shearer Operating in a U.S. Coal Seam. In Proceedings of the 15th North American Mine Ventilation Symposium, Blacksburg, VA, USA, 21–25 June 2015.
79. Geortz, B.J.; Brune, J.; McDaniel, S.; Rockley, T.; Barreto, F.S.; Demontigny, N. Development of a Mine Dust Sampling Instrument for use in Underground Coal Mines. In Proceedings of the 15th North American Mine Ventilation Symposium, Blacksburg, VA, USA, 21–25 June 2015.
80. Kumar, A.; Arya, S.; Wedding, W.C.; Novak, T. Examination of Capture Efficacies of a Shearer Mounted Flooded Bed Dust Scrubber Using Experiments and Computational Fluid Dynamics (CFD) Modeling on a Reduced Scaled Model. In Proceedings of the 16th North American Mine Ventilation Symposium, Golden, CO, USA, 17–22 July 2017.
81. Zhou, G.; Zhang, Q.; Hu, Y.; Gao, D.; Wang, S.; Sun, B. Dust removal effect of negatively-pressured spraying collector for advancing support in fully mechanized coal mining face: Numerical simulation and engineering application. *Tunn. Undergr. Space Technol.* **2020**, *95*, 103149. [CrossRef]
82. Arya, S.; Novak, T.; Sottile, J. Experimental and Numerical Investigation of the Effect of Integration of a Flooded-Bed Scrubber into a Longwall Shearer on Airflow along a Coal Mine Longwall Face. *Appl Sci.* **2021**, *11*, 3617. [CrossRef]
83. Chen, D.; Nie, W.; Cai, P.; Liu, Z. The diffusion of dust in a fully-mechanized mining face with a mining height of 7m and the application of wet dust-collecting nets. *J. Clean. Prod.* **2018**, *205*, 463–476. [CrossRef]
84. Xiu, Z.; Nie, W.; Yan, J.; Chen, D.; Cai, P.; Liu, Q.; Du, T.; Yang, B. Numerical simulation study on dust pollution characteristics and optimal dust control air flow rates during coal mine production. *J. Clean. Prod.* **2020**, *248*, 119197. [CrossRef]
85. Hurtado, J.P.; Reyes, G.; Vargas, J.P.; Acuna, E. A Computational Fluid Dynamic Study of Developed Parallel Stations for Primary Fans. *Processes* **2021**, *9*, 1607. [CrossRef]
86. Zhelnin, M.; Kostina, A.; Plekhov, O.; Zaitsev, A.; Olkhovskiy, D. Numerical Simulation on Temperature and Moisture Fields Around Cooling Towers Used in Mine Ventilation System. *Fluids* **2022**, *7*, 317. [CrossRef]
87. Adjiski, V. Possibilities for simulating the smoke rollback effect in underground mines using CFD software. *GeoSci. Eng.* **2014**, *2*, 8–18. [CrossRef]
88. Lee, C.; Kim, H. CFD Analysis of Truck Fire in Large-Opening Limestone Mine. In Proceedings of the 15th North American Mine Ventilation Symposium, Blacksburg, VA, USA, 21–25 June 2015.

89. Yuan, Y.; Smith, A.C. Numerical Study on the Effects of Water Spray Characteristics on Suppression of Conveyor Belt Fires. In Proceedings of the 15th North American Mine Ventilation Symposium, Blacksburg, VA, USA, 21–25 June 2015.
90. Zhou, Z.; Cui, Y.; Tian, L.; Chen, J.; Pan, W.; Yang, S.; Hu, P. Study of the Influence of Ventilation Pipeline Setting on Cooling Effects in High-Temperature Mines. *Energies* **2019**, *12*, 4074. [CrossRef]
91. Huang, R.; Shen, X.; Wu, E.; Li, Z. Study on the influence law of ventilation conditions on heat loss in a roadway of high altitude mine. *Numer. Heat Transfer.* **2020**, *77*, 69–79. [CrossRef]
92. Xin, S.; Wang, W.; Zhang, N.; Zhang, C.; Yuan, S.; Li, H. Comparative studies on control of thermal environment in development headings using force/exhaust overlap ventilation systems. *J. Build. Eng.* **2021**, *38*, 102227. [CrossRef]
93. Fernánez-Alaiz, F.; Castañón, A.M.; Gómez-Fernández, F.; Bernardo-Sánchez, A.; Bascompta, M. Analysis of the Fire Propagation in a Sublevel Coal Mine. *Energies* **2020**, *13*, 3754. [CrossRef]
94. Fernánez-Alaiz, F.; Castañón, A.M.; Gómez-Fernández, F.; Bernardo-Sánchez, A.; Bascompta, M. Mine Fire Behavior under Different Ventilation Conditions: Real-Scale Tests and CFD Modeling. *Appl. Sci.* **2020**, *10*, 3380. [CrossRef]